FINITE ELEMENT MODELING OF CONCRETE EXPANSION AND CONFINEMENT

By F. J. Vecchio[1]

ABSTRACT: The lateral expansion of concrete subjected to compression (i.e., the Poisson effect) is shown to be a significant factor influencing the behavior of reinforced concrete elements in tension-compression states in which the principal tensile strain is relatively small. A method is presented by which concrete lateral expansion can be incorporated into a nonlinear finite element algorithm. The formulations presented presume the use of a secant-stiffness–based solution procedure, involving the concept of material prestrains. Material behavior models are described for nonlinear concrete expansion, strength reduction due to transverse cracking, strength enhancement due to confinement, and pre- and postultimate stress-strain response. The accuracy of the formulations are examined through finite element analyses of a number of shear panels and shear walls previously tested. It is shown that the inclusion of concrete lateral expansion can, in some cases, significantly alter the computed response of an element or structure. Further, it is shown that the consideration of expansion and confinement effects generally results in a significant improvement in the accuracy of the analysis.

INTRODUCTION

The modified compression field theory (MCFT) was proposed several years ago as a simple analytical model for predicting the load-deformation response of reinforced concrete elements subjected to in-plane shear and normal stresses (Vecchio and Collins 1986). The model considered equilibrium and compatibility conditions within an element in terms of average stresses and average strains. Local stress conditions at crack locations were also considered. New constitutive relations were proposed for cracked concrete, based on extensive test data, reflecting significant influences due to compression softening and tension-stiffening mechanisms.

The formulations of the MCFT were subsequently incorporated into a nonlinear finite element algorithm (Vecchio 1989). Accordingly, cracked reinforced concrete was treated as an orthotropic material using a smeared, rotating crack modeling approach. The solution procedure used was based on a secant-stiffness formulation, giving good numerical stability and providing much freedom in the definition of material behavior models. The finite element formulations were later further developed to permit the consideration of prestrains in the component materials (Vecchio 1990).

Subsequent to the original formulation, experimental data have shown the MCFT to somewhat overestimate the compression-softening effect in elements experiencing relatively low tensile strains. In reexamining the original test panels (Vecchio and Collins 1986), this is seen to be the case in panels subjected to combined shear and biaxial compression, and in panels loaded in pure shear containing a high percentage of transverse reinforcement that did not yield. As well, an overestimation of the compression

[1]Assoc. Prof., Dept. of Civ. Engrg., Univ. of Toronto, 35 St. George St., Toronto, Canada M5S 1A4.

Note. Discussion open until February 1, 1993. To extend the closing date one month, a written request must be filed with the ASCE Manager of Journals. The manuscript for this paper was submitted for review and possible publication on May 12, 1991. This paper is part of the ***Journal of Structural Engineering***, Vol. 118, No. 9, September, 1992. ©ASCE, ISSN 0733-9445/92/0009-2390/$1.00 + $.15 per page. Paper No. 1857.

softening has been noted for some panels subsequently tested at the University of Toronto and elsewhere, particularly in panels in which the principal tension and compression directions coincided with the orientation of the reinforcement. This led to the realization that concrete expansion normal to the compression (i.e., Poisson effect), hitherto not accounted for in the MCFT, was a significant factor in elements experiencing relatively low tensile straining.

In this paper, methods for the inclusion of concrete expansion in nonlinear finite element analyses are discussed. The concept of material prestrains is extended to accommodate modeling of the Poisson effect, and preliminary material behavior models are described. The finite element analyses presented herein examine the relative significance of accounting for concrete lateral expansion, and the resulting influence on the accuracy of compression field type analyses.

Finite Element Formulation

A linear elastic orthotropic material, in the condition of plane stress, is described in the principal stress directions by the stiffness matrix

$$\mathbf{D} = \frac{1}{1 - \nu_{12}\nu_{21}} \begin{bmatrix} E_1 & \nu_{12}E_1 & 0 \\ \nu_{21}E_2 & E_2 & 0 \\ 0 & 0 & (1 - \nu_{12}\nu_{21})G_{12} \end{bmatrix} \quad \ldots\ldots\ldots\ldots\ldots\ldots (1)$$

where the shear modulus G_{12} is given by

$$G_{12} \simeq \frac{E_1E_2}{E_1(1 + \nu_{12}) + E_2(1 + \nu_{21})} \quad \ldots\ldots\ldots\ldots\ldots\ldots\ldots\ldots (2)$$

(Weaver and Johnson 1984). To maintain symmetry in the stiffness matrix, the following condition must be satisfied:

$$\frac{E_2}{E_1} = \frac{\nu_{12}}{\nu_{21}} \quad \ldots\ldots\ldots\ldots\ldots\ldots\ldots\ldots\ldots\ldots\ldots\ldots\ldots\ldots\ldots\ldots\ldots\ldots (3)$$

Consider a concrete element subjected to biaxial stress conditions such that $f_{c2} < f_{c1}$ [see Fig. 1(*a*)]. It has been common to assume, in orthotropic formulations of cracked reinforced concrete, that the Poisson effects are negligible (e.g., Vecchio 1989, 1990; Hu and Schnobrich 1990). Thus, with $\nu_{12} = \nu_{21} = 0$, the stiffness matrix for concrete becomes

$$\mathbf{D}'_c = \begin{bmatrix} \bar{E}_{c1} & 0 & 0 \\ 0 & \bar{E}_{c2} & 0 \\ 0 & 0 & \bar{G}_c \end{bmatrix} \quad \ldots\ldots\ldots\ldots\ldots\ldots\ldots\ldots\ldots\ldots\ldots\ldots\ldots\ldots\ldots\ldots\ldots\ldots (4)$$

This assumption leads to relatively simple and reasonably accurate modeling of concrete behavior in tension-compression states. However, in biaxial compression states (i.e., when concrete is uncracked), or in cases where the tensile strains in cracked concrete are relatively small, the lateral expansion of concrete arising from Poisson effects can represent a significant portion of the total strains.

The constitutive response of concrete in compression is characterized by a progressively softening stress-strain curve [see Fig. 1(*b*)]. Further, due to mechanisms related to internal microcracking, concrete exhibits a progressively higher proportion of lateral expansion as compression is increased

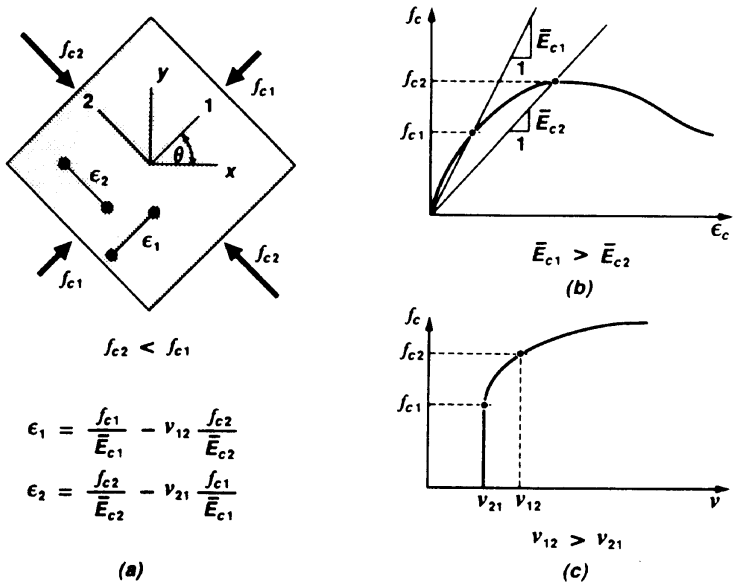

FIG. 1. Concrete Element Loaded in Biaxial Compression: (*a*) Definition of Element Strains; (*b*) Variations in Modulus of Elasticity; (*c*) Variations in Poisson Ratio

[see Fig. 1(*c*)]. Thus, for the condition where $f_{c2} < f_{c1}$, it is generally true that $\bar{E}_{c2} < \bar{E}_{c1}$ and $\nu_{12} > \nu_{21}$. This behavior is in direct conflict with the requirements of (3). Thus, an elastic orthotropic formulation for concrete in accordance with the stiffness formulation in (1) cannot accurately represent behavior in which expansion effects are significant. A means by which this numerical difficulty can be circumvented lies in the use of a modeling concept developed for material prestrains.

The finite element formulations developed previously permitted the inclusion of prestrain effects in the component materials of a reinforced concrete element. This enabled the consideration of prestressing in reinforcement, shrinkage, or expansion of concrete, thermal expansion of either concrete or reinforcement, or other types of strain offset effects. For concrete, a prestrain matrix $\boldsymbol{\varepsilon}_c^o$ was defined relative to x, y system

$$\boldsymbol{\varepsilon}_c^o = \lfloor\, \varepsilon_{cx}^o \varepsilon_{cy}^o \gamma_{cxy}^o \,\rfloor \quad \ldots\ldots (5)$$

accounting for all nonstress-related straining. The prestrains ε_{cx}^o, ε_{cx}^o, and γ_{cxy}^o were then rigorously included in the finite element formulations (i.e., in determining stiffness factors and prestrain joint forces). The analysis procedure is fully described in Vecchio (1990). It is adapted here to include expansions related to Poisson effects.

Expansion prestrains are most conveniently determined with respect to the principal axes; i.e.

$$\varepsilon_{c1}^o = -\nu_{12}\frac{f_{c2}}{\bar{E}_{c2}} \quad \ldots\ldots (6)$$

$$\varepsilon_{c2}^o = -\nu_{21}\frac{f_{c1}}{\bar{E}_{c1}} \quad \ldots\ldots (7)$$

Transforming the strains to the x, y reference system yields the following relationships:

$$\varepsilon^o_{cx} = \varepsilon^o_{c1} \frac{(1 + \cos 2\theta)}{2} + \varepsilon^o_{c2} \frac{(1 - \cos 2\theta)}{2} \quad \ldots\ldots (8)$$

$$\varepsilon^o_{cy} = \varepsilon^o_{c1} \frac{(1 - \cos 2\theta)}{2} + \varepsilon^o_{c2} \frac{(1 + \cos 2\theta)}{2} \quad \ldots\ldots (9)$$

$$\gamma^o_{cxy} = \varepsilon^o_{c1} \sin 2\theta - \varepsilon^o_{c2} \sin 2\theta \quad \ldots\ldots (10)$$

where θ defines the orientation of the principal axes [see Fig. 1(*a*)].

To optimize the numerical efficiency of the calculation procedure, as much of the expansion effect as possible is included directly in the formulation of the stiffness matrix. Only the portion that cannot be accounted for directly is modeled in terms of prestrains. Thus, assume

$$\varepsilon^o_{c2} = 0 \quad \ldots\ldots (11)$$

Now, consider the Poisson ratio ν_{12} to be composed of an elastic component, ν^e_{12}, and a residual component, ν^*_{12}. The elastic component will be such as to satisfy the orthotropic requirements of (3); thus

$$\nu^e_{12} = \nu_{21} \cdot \frac{\bar{E}_{c2}}{\bar{E}_{c1}} \quad \ldots\ldots (12)$$

and

$$\nu^*_{12} = \nu_{12} - \nu^e_{12} \quad \ldots\ldots (13)$$

The component of expansion in the 1-direction, due to the stress f_{c2}, that must be modeled as a prestrain is

$$\varepsilon^o_{c1} = -\nu^*_{12} \frac{f_{c2}}{\bar{E}_{c2}} \quad \ldots\ldots (14)$$

The remaining expansion in the 1-direction, and the whole of the expansion in the 2-direction, is accounted for in the symmetrical stiffness matrix

$$\mathbf{D}'_c = \frac{1}{1 - \nu^e_{12}\nu_{21}} \begin{bmatrix} \bar{E}_{c1} & \nu^e_{12}\bar{E}_{c1} & 0 \\ \nu_{21}\bar{E}_{c2} & \bar{E}_{c2} & 0 \\ 0 & 0 & (1 - \nu^e_{12}\nu_{21})\bar{G}_{c12} \end{bmatrix} \quad \ldots\ldots (15)$$

where

$$\bar{G}_{c12} = \frac{\bar{E}_{c1} \cdot \bar{E}_{c2}}{\bar{E}_{c1}(1 + \nu^e_{12}) + \bar{E}_{c2}(1 + \nu_{21})} \quad \ldots\ldots (16)$$

An iterative solution procedure is required for nonlinear finite element analysis based on this approach. The algorithm described in Vecchio (1990) remains valid if $\boldsymbol{\varepsilon}^o_c$ and $\mathbf{D}'_c$ are modified as discussed. The procedure is also valid in tension-compression cases, and for both cracked and uncracked conditions.

Material Modeling

The formulations described were implemented in a two-dimensional nonlinear finite element program based on a secant-stiffness formulation (Vecchio 1989, 1990). The procedure was enhanced to nominally account for triaxial stress effects, in membrane-type structures, arising from expansion

in the out-of-plane direction restrained by reinforcement. Given the out-of-plane reinforcement ratio ρ_z, and recognizing that the compressive stresses in the out-of-plane direction are likely to be relatively small, these stresses were approximated by

$$f_{cz} = -\rho_z \cdot f_{sz} \quad \ldots\ldots (17)$$

where

$$f_{sz} = E_s \cdot \varepsilon_{cz} \gtrless f_{yz} \quad \ldots\ldots (18)$$

If the out-of-plane reinforcement is not yielding

$$\varepsilon_{cz} = \frac{E_{cn}}{E_{cn} + \rho_z \cdot E_s} \cdot \left(-\nu_{12} \cdot \frac{f_{c2}}{\bar{E}_{c2}} - \nu_{21} \frac{f_{c1}}{\bar{E}_{c1}} \right) \quad \ldots\ldots (19)$$

otherwise

$$\varepsilon_{cz} = -\frac{\rho_z \cdot f_{yz}}{E_{cn}} - \nu_{12} \frac{f_{c2}}{\bar{E}_{c2}} - \nu_{21} \frac{f_{c1}}{\bar{E}_{c1}} \quad \ldots\ldots (20)$$

The modulus of elasticity of concrete in the out-of-plane direction, E_{cn}, was considered to be constant and equal to $2f'_c/\varepsilon_o$.

To complete the implementation of expansion and confinement effects, material models were required for strength degradation due to cracking, for strength enhancement due to confinement (i.e., biaxial or triaxial compression), for pre- and postpeak stress-strain response, and for concrete lateral expansion. The models tentatively used are as follows.

For cracked concrete subjected to a tension-compression stress state, the constitutive modeling was done according to the modified compression field theory (Vecchio and Collins 1986). The strength reduction factor β for concrete in compression, shown in Fig. 2(*a*), is given by

$$\beta = \frac{1}{0.85 - 0.27 \frac{\varepsilon_{c1}}{\varepsilon_{c2}}} \gtrless 1.0 \quad \ldots\ldots (21)$$

where ε_{c2} and ε_{c1} = the strains in the principal compressive and principal tensile directions, respectively. Thus, the peak compressive stress attainable is

$$f_p = \beta \cdot f'_c \quad \ldots\ldots (22)$$

occurring at the peak strain

$$\varepsilon_p = \beta \cdot \varepsilon_o \quad \ldots\ldots (23)$$

The stress-strain relationship, illustrated in Fig. 2(*b*), is

$$f_{c2} = -f_p \left[2 \left(\frac{\varepsilon_{c2}}{\varepsilon_p} \right) - \left(\frac{\varepsilon_{c2}}{\varepsilon_p} \right)^2 \right], \quad 0 > \varepsilon_{c2} > \varepsilon_p \quad \ldots\ldots (24)$$

$$f_{c2} = -f_p \left[1 - \left(\frac{\varepsilon_{c2} - \varepsilon_p}{2\varepsilon_o - \varepsilon_p} \right)^2 \right], \quad \varepsilon_p > \varepsilon_{c2} > -2\varepsilon_o \quad \ldots\ldots (25)$$

The relationship for concrete in tension, shown in Figure 2(*c*), is given as

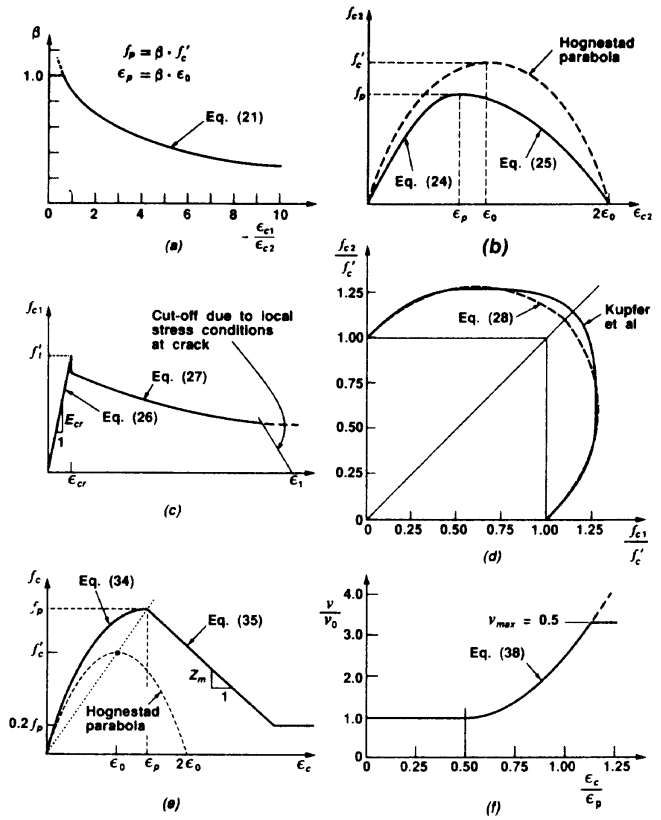

FIG. 2. Material Models for Concrete: (*a*) Compression Softening Parameter; (*b*) Constitutive Response of Cracked Concrete in Compression; (c) Constitutive Response of Cracked Concrete in Tension; (*d*) Strength Enhancement due to Biaxial Compression; (e) Constitutive Response of Confined Concrete; (*f*) Poisson Ratio

$$f_{c1} = E_{cn} \cdot \varepsilon_{c1}, \quad 0 < \varepsilon_{c1} < \varepsilon_{cr} \quad \ldots\ldots (26)$$

$$f_{c1} = \frac{f'_t}{1 + \sqrt{200} \cdot \varepsilon_{c1}}, \quad \varepsilon_{c1} > \varepsilon_{cr} \quad \ldots\ldots (27)$$

and is subject to reduction based on local conditions at crack locations.

For concrete in a biaxial compression state, strength enhancement was modeled using a relationship approximating the Kupfer et al. (1969) model [see Fig. 2(*d*)]. The strength enhancement factor for concrete in the 2-direction, arising from the stress f_{c1} acting in the 1-direction, is given by

$$K_c = 1 + 0.92\left(\frac{-f_{c1}}{f'_c}\right) - 0.76\left(\frac{-f_{c1}}{f'_c}\right)^2 \quad \ldots\ldots (28)$$

The peak stress, f_p, and strain at peak stress, ε_p, are

$$f_p = K_c \cdot f'_c \quad \ldots\ldots (29)$$

$$\varepsilon_p = K_c \cdot \varepsilon_o \quad \ldots\ldots (30)$$

The strength enhancement factor for concrete in the 1-direction, due to the stress f_{c2}, is similarly determined by substituting f_{c2} for f_{c1} in (28).

Strength enhancement effects and increased ductility are particularly significant in the case of triaxial compression. To determine strength increases in the direction of the largest compressive stress (i.e., f_{c3}), given the two

normal compressive stresses f_{c1} and f_{c2} (assume $f_{c2} < f_{c1}$), the relationship used was

$$K_c = 4.1\left(\frac{f_{cb}}{f'_c}\right) + \left[1 + 0.92\left(\frac{f_{cn}}{f'_c}\right) - 0.76\left(\frac{f_{cn}}{f'_c}\right)^2\right] \quad \ldots\ldots (31)$$

where

$$f_{cb} = -f_{c1} \quad \ldots\ldots (32)$$

and

$$f_{cn} = -(f_{c2} - f_{c1}) \quad \ldots\ldots (33)$$

The first term in (31) represents the strength enhancement effect noted in spiral columns by Richart et al. (1928). Again, the peak stress and peak strain are determined by (29) and (30). To evaluate strength enhancements in the other two directions, f_{c1}, f_{c2}, and f_{c3} are interchanged accordingly.

The constitutive response model for biaxially and triaxially compressed concrete was based on a liberal modification of the modified Kent-Park model (Scott et al. 1982)[see Fig. 2(*e*)]. The relationships used were

$$f_{c3} = -f_p\left[2\left(\frac{\varepsilon_{c3}}{\varepsilon_p}\right) - \left(\frac{\varepsilon_{c3}}{\varepsilon_p}\right)^2\right], \quad 0 > \varepsilon_{c3} > \varepsilon_p \quad \ldots\ldots (34)$$

$$f_{c3} = -f_p[1 + Z_m(\varepsilon_{c3} - \varepsilon_p)] \not> 0.2f_p, \quad \varepsilon_{c3} < \varepsilon_p \quad \ldots\ldots (35)$$

where

$$Z_m = \frac{0.5}{\dfrac{3 + 0.29f'_c}{145f'_c - 1000}} + \frac{2f_{cl} + f_{cn}}{450} + \varepsilon_p \quad \ldots\ldots (36)$$

Concrete in compression exhibits a lateral expansion characterized by a progressively increasing Poisson ratio. At compressive stresses near failure, the Poisson ratio can exceed 0.5 (i.e., volume increasing). The behavior model tentatively used for the Poisson effect [see Fig. 2(*f*)], is given by

$$\nu_{12} = \nu_o, \quad 0 > \varepsilon_{c2} > \frac{\varepsilon_p}{2} \quad \ldots\ldots (37)$$

$$\nu_{12} = \nu_o\left[1 + 1.5\left(\frac{2\varepsilon_{c2}}{\varepsilon_p} - 1\right)^2\right] \not> 0.5, \quad \frac{\varepsilon_p}{2} > \varepsilon_{c2} \quad \ldots\ldots (38)$$

where ν_o = the initial value of the Poisson ratio. The expansion in the 2-direction due to the stress f_{c1} (i.e., ν_{21}) is similarly found from (38) by substituting ε_{c1} for ε_{c2}. For concrete in tension, prior to cracking, the Poisson ratio was considered constant at ν_o. After cracking, the Poisson ratio was equated to zero for expansion normal to the tensile direction only (i.e., $\nu_{21} = 0$, $\nu_{12} \neq 0$).

Analysis of Shear Panels

To obtain an indication of the importance of expansion and confinement effects, and their impact on the accuracy of compression field-type analyses,

a number of the shear panels that had been originally tested (Vecchio and Collins 1986) were reanalyzed. The panels chosen for investigation (see Table 1) were among those that experienced a shear or crushing failure of the concrete prior to yielding of the longitudinal reinforcement. These panels were subdivided into two groups: (1) Panels loaded in pure shear, in which ρ_x equalled 1.79% and ρ_y varied from 0 to 1.79%; and (2) panels loaded in combined shear and biaxial normal stresses, in which ρ_x and ρ_y both equalled 1.79%. All of the test panels considered achieved, during testing, ultimate and postultimate load conditions (i.e., no premature or edge failures).

For finite element analysis, a single-element model with smeared reinforcement was used. The panel parameters and material properties used in the modeling are given in Table 1. (It should be noted that none of the panels contained out-of-plane reinforcement.) Two sets of analyses were performed using the nonlinear program TRIX, alternatively considering and not considering expansion or confinement effects.

Comparisons between the two theoretical strengths determined for each of the panels, against the experimentally observed strengths, are given in Fig. 3. It can be seen that including the effects of expansion in the analyses generally resulted in an increase in the predicted strength of the panels. The influence was minimal in panels experiencing large tensile strains (i.e., in panels having $\rho_y << \rho_x$, experiencing yielding of the transverse reinforcement). The influence became progressively more pronounced in panels sustaining smaller transverse tensile strains (i.e., in panels in which the transverse reinforcement did not yield; PV22, PV23, PV25, PV27, PV28). The increase in predicted strength was the result of the lateral expansion of concrete normal to the principal compression (i.e., $\nu_{12} f_{c2}/\bar{E}_{c2}$) accounting for a significant reduction in the net principal tensile strain, ε_1. This, in turn, partially negated the compression softening effect predicted by (21) and (22).

In comparing the experimental results with the predictions made with and without expansion, a slight improvement in the accuracy of the analyses was realized by accounting for expansion. For the 11 panels considered, the mean of the ratio of experimental to theoretical strength changed from 1.03 to 0.98. More importantly, the coefficient of variation was improved from 8.8% to 6.9%, reflecting significantly less scatter in the predictions (see Fig. 4). The indication is that concrete expansion is an essential part of the behavior of concrete, and should be accounted for. However, it should be realized that the compression softening model used was the one originally deduced from the test data neglecting any Poisson effects. A revised model currently being formulated, compensating for Poisson-related strains, will no doubt yield improved accuracy.

The inclusion of concrete expansion also resulted in changes in the predicted load-deformation responses of the panels. The responses were generally unaffected at low and intermediate load levels, but exhibited increases in strength and stiffness at near-ultimate conditions. The increases, however, were relatively minor in elements experiencing large transverse tensile strains.

All of the panels considered herein were ones subjected to cracked tension-compression states. The influence of expansion and confinement is of even greater significance in elements subjected to biaxial or triaxial compression states. This became evident in the results of analyses performed on shear walls.

TABLE 1. Panel Specimen Properties

Panel (1)	f'_c (MPa) (2)	f'_t (MPa) (3)	E_c (MPa) (4)	ρ_x (%) (5)	f_{yx} (MPa) (6)	ρ_y (%) (7)	f_{yy} (MPa) (8)	Loading			v_{Uexp} (MPa) (12)
								σ_x (9)	σ_y (10)	τ_{xy} (11)	
PV10	14.5	1.25	10,750	1.785	276	1.000	276	0	0	1	3.97
PV12	16.0	1.32	12,800	1.785	469	0.446	269	0	0	1	3.13
PV18	19.5	1.45	17,700	1.785	431	0.315	412	0	0	1	3.04
PV19	19.0	1.44	17,700	1.785	458	0.719	299	0	0	1	3.95
PV20	19.6	1.46	21,800	1.785	460	0.885	297	0	0	1	4.26
PV21	19.5	1.46	21,700	1.785	458	1.296	302	0	0	1	5.03
PV22	19.6	1.46	19,600	1.785	458	1.524	420	0	0	1	6.07
PV23	20.5	1.50	20,500	1.785	518	1.785	518	−0.39	−0.39	1	8.87
PV25	19.2	1.45	21,400	1.785	466	1.785	466	−0.69	−0.69	1	9.12
PV27	20.5	1.50	21,600	1.785	442	1.785	442	0	0	1	6.35
PV28	19.0	1.44	20,500	1.785	483	1.785	483	0.32	0.32	1	5.80

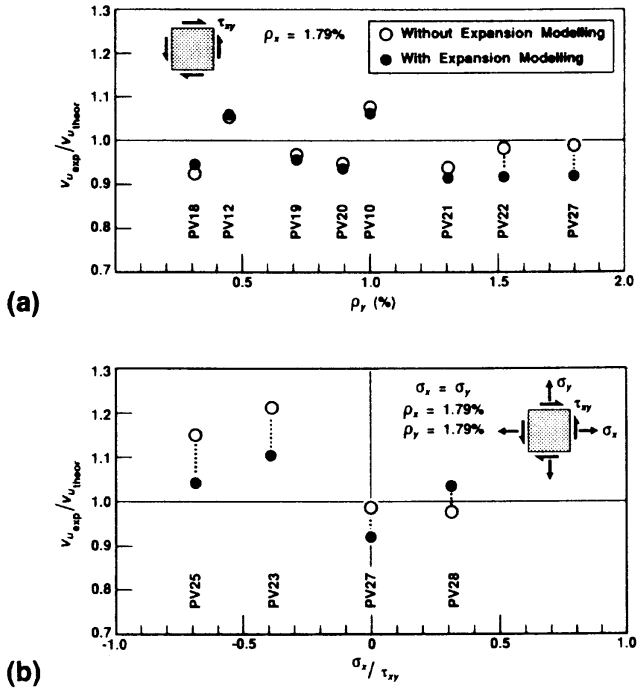

FIG. 3. Comparison of Predicted to Observed Strength of Shear Panels: (*a*) Panels Loaded in Pure Shear; (*b*) Panels Loaded in Shear and Biaxial Normal Stress

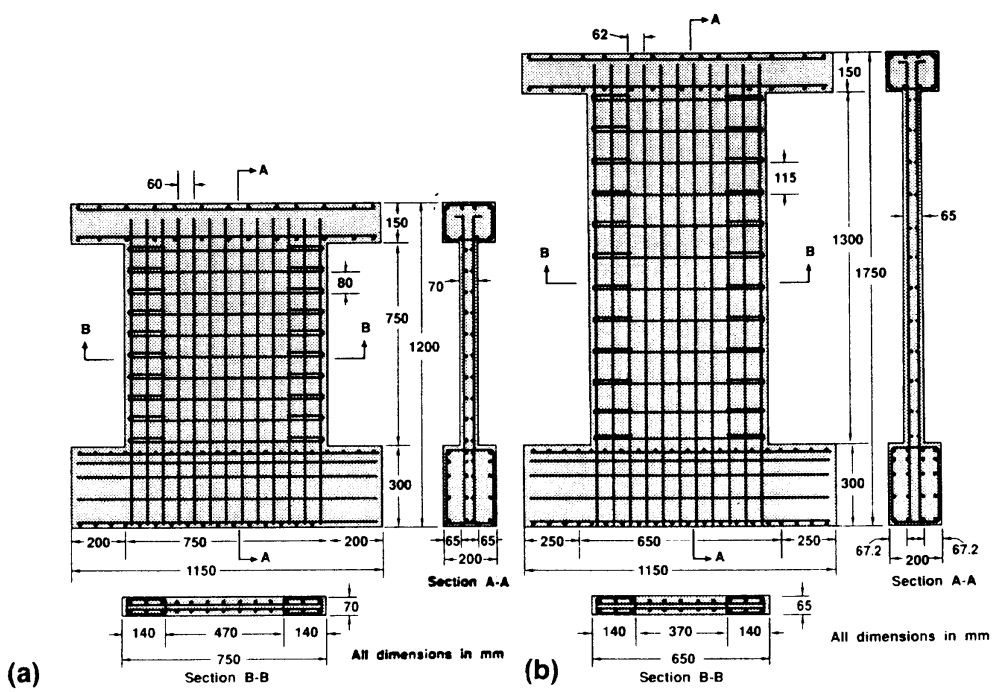

FIG. 4. Details of Shear Walls Tested by Lefas et al. (1990); (*a*) Type-I Walls; (*b*) Type-II Walls

Analysis of Shear Walls

The shear walls chosen for analytical study were walls recently tested by Lefas et al. (1990). The test program comprised 13 large-scale walls tested under various conditions of axial load and monotonically increasing lateral load. The wall geometries were of two types: The type-I walls were relatively

squat, having a height-to-width ratio of 1.0 [see Fig. 4(*a*)]; the type-II walls were more slender, with a height-to-width ratio of 2.0 [see Fig. 4(*b*)]. In both cases, the walls were of rectangular cross section. A thickened and heavily reinforced base structure and a top spreader beam, cast integrally with the walls, were used for load transfer.

Generally, both types of walls were reinforced in the vertical and horizontal directions, in accordance with ACI 318 specifications. (In two of the walls, SW17 and SW26, the horizontal reinforcement ratio was reduced to test the validity of the shear design procedures.) The vertical reinforcement typically consisted of two layers of 8-mm-diameter deformed bars at 60-mm spacing in the type-I walls, and at 62-mm spacing in the type-II walls. The horizontal reinforcement consisted of 6.25-mm-diameter bars at 80-mm spacing in the type-I walls, and at 115-mm spacing in the type-II walls. In both wall types, a 140-mm-wide concealed column was effectively formed at each edge of the wall by the inclusion of closed ties fabricated from 4-mm-diameter bar.

The walls were subjected to constant axial loads combined with horizontal loads that were monotonically increased until failure. The loads were applied through the top spreader beam. The constant axial loads applied are given in Table 2.

The walls exhibited a strong, ductile behavior, developing strengths greater than expected. The concrete at the base of the walls, and within the concealed columns, was well confined. Lefas et al. (1990) reported the development of triaxial compressive stress conditions in these zones, and attributed the high shear resistance of the walls to this state of stress.

Finite element modeling was undertaken for the two series of walls tested. The walls were modeled for membrane stress analysis using low-powered linear displacement rectangular elements. A 155-element mesh was used to present the type-I walls, and a 140-element mesh was used for the type-II walls (see Fig. 5). Loads acting on the wall structures were applied as nodal forces along the top spreader beam. The nodes along the lower edge of the base structure were assumed fixed.

TABLE 2. Wall Specimen Properties—Concrete

Wall[a] (1)	Type (2)	Axial load (kN) (3)	f'_c (MPa) (4)	f'_t (MPa) (5)	E_c (MPa) (6)
SW11	I	0	44.5	2.20	33,350
SW12	I	230	45.6	2.23	33,750
SW13	I	355	34.5	1.94	29,350
SW14	I	0	35.8	1.97	29,900
SW15	I	185	36.8	2.00	30,300
SW16	I	460	44.0	2.20	33,150
SW17	I	0	41.1	2.12	32,050
SW21	II	0	36.4	2.00	30,150
SW22	II	182	43.0	2.16	32,800
SW23	II	343	40.6	2.10	31,850
SW24	II	0	41.1	2.12	32,050
SW25	II	325	38.3	2.04	30,950
SW26	II	0	25.6	1.67	25,300

[a] $\nu_o = 0.15$ assumed for all walls.

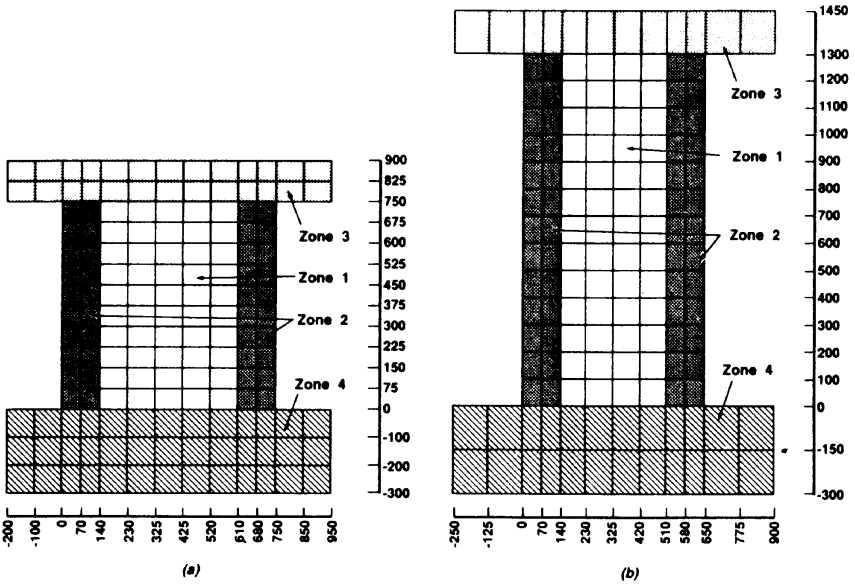

FIG. 5. Finite Element Modeling of Walls (See Tables 3 and 4 for Concrete and Reinforcement Properties): (*a*) Type-I Walls; (*b*) Type-II Walls

The concrete material properties, as used in the modeling, are reported in Table 2. The concrete cylinder strength was taken as 85% of the cube strength reported by Lefas et al. (1990). The tensile strength and modulus of elasticity were estimated from the cylinder strength; $f_t' = 0.33\sqrt{f_c'}$ and $E_c = 5{,}000\sqrt{f_c'}$, respectively. The Poisson ratio was taken as 0.15. For the reinforcement, the yield strengths of the 8-mm-, 6.25-mm-, and 4-mm-diameter bars were 470 MPa, 520 MPa, and 420 MPa, respectively. The modulus of elasticity used was 210,000 MPa. Being cold drawn, the reinforcement was assumed to have a strain hardening modulus of 10,000 MPa beginning at a strain of 2.5×10^{-3} mm/mm.

The wall reinforcement was modeled in a smeared manner. Four zones were distinguishable in each wall type in terms of reinforcement ratios and wall thicknesses: wall interior zone, wall edge zone, spreader beam, and base structure (see Fig. 5). The reinforcement ratios assigned to elements in each of these zones are given in Table 3.

Nonlinear finite element analyses were conducted using program TRIX. Expansion and confinement effects were taken into account using the formulations and material behavior models previously described. (It should be noted that all modeling decisions were made and data input files created, for all the walls, before any analysis was made. Further, each wall was analyzed once only. Thus, the results obtained were essentially true predictions.)

For all walls, the predicted sequence of failure involved flexural-shear cracking, followed by yielding of the vertical reinforcement on the tension side, ending with crushing of the concrete near the base on the compression side. Elements near the compression base developed significant levels of triaxial compression. In no wall did the stresses in the horizontal reinforcement approach yield. All these aspects of behavior agreed well with the experimentally observed response.

The ultimate loads obtained from the theoretical analyses are compared with the experimental values in Table 4. It can be seen that the strengths of both the type-I and type-II walls were predicted very accurately. For the

TABLE 3. Wall Specimen Properties—Reinforcement

Zone (1)	t (mm) (2)	ρ_x (%) (3)	f_{yx} (MPa) (4)	ρ_y (%) (5)	f_{yy} (MPa) (6)	ρ_z (%) (7)	f_{yz} (MPa) (8)
			(*a*) Type-I walls				
1	70	1.095[a]	520	2.138	470	—	—
2	70	1.095[a]/0.448	520/420	3.076	470	1.200	420
3	200	0.818	520	0.837/0.209	470/420	0.279	420
4	200	1.675	520	0.837/0.209	470/420	0.140	420
			(*b*) Type-II walls				
1	65	0.820[b]	520	2.090	470	—	—
2	65	0.820[b]/0.336	520/420	3.312	470	0.900	420
3	200	0.818	520	0.810/0.203	470/420	0.270	420
4	200	1.022	520	0.810/0.203	470/420	0.135	420

[a]0.365 in wall SW17.
[b]0.410 in wall SW26.

TABLE 4. Wall Specimen Results

Wall (1)	$F_{u\text{exp}}$ (kN) (2)	Without Expansion Modeling		With Expansion Modeling	
		$F_{u\text{theor}}$ (MPa) (3)	Experimental/ Theoretical (4)	$F_{u\text{theor}}$ (MPa) (5)	Experimental/ Theoretical (6)
SW11	260	252	1.032	285	0.912
SW12	340	292	1.164	345	0.986
SW13	330	260	1.269	305	1.082
SW14	265	226	1.173	280	0.946
SW15	320	252	1.270	320	1.000
SW16	355	310	1.145	360	0.986
SW17	247	232	1.065	260	0.950
SW21	127	116	1.095	124	1.025
SW22	150	140	1.071	152	0.987
SW23	180	148	1.216	162	1.111
SW24	120	120	1.000	126	0.952
SW25	150	144	1.042	150	1.000
SW26	123	99	1.242	112	1.098
Mean	—	—	1.137	—	1.003
COV	—	—	0.082	—	0.061

13 walls analyzed, the ratio of the experimental to predicted strength had a mean of 1.00 and a coefficient of variation of 6.1%.

The predicted load-deformation responses also compared well with the experimental results. Shown in Fig. 6, as representative examples, are the theoretical and experimental horizontal deflections at the top of walls SW16 and SW25. Generally, the deflections were predicted reasonably well at all stages of loading. There was a tendency, however, to underestimate deflections in the type-I walls. As well, at ultimate loads, the experimental results demonstrated a more ductile response, whereas the force-controlled analyses reflected a more brittle crushing failure.

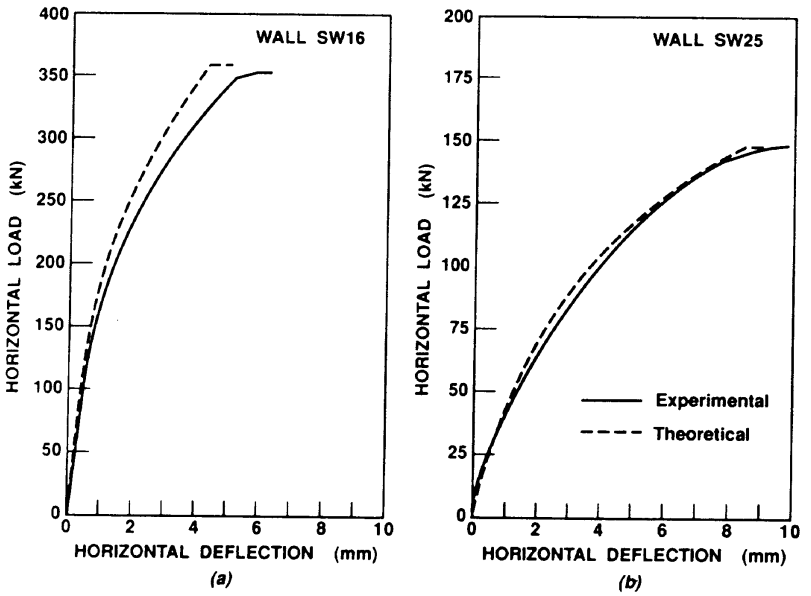

FIG. 6. Comparison of Predicted and Observed Load-Deformation Response of Shear Walls: (*a*) Wall SW16; (*b*) Wall SW25

Other aspects of behavior were also examined, including crack patterns, stresses in the reinforcement, surface strains, and failure modes. Again, good correlation was found between the experimental and analytical results.

The finite element analyses provided useful information regarding the distribution of stresses within the walls. Consider, for example, the principal compressive stress and normal shear stress distributions that developed across the base of wall SW16 at ultimate load (F_H = 360 kN). The principal compressive stress f_{c3} rose from essentially zero on the tension face to a value of -68.3 MPa ($1.55f'_c$) on the compression face. In the outermost element, the two normal stresses that developed as a result of expansion and confinement were $f_{c1} = f_{cz} = -3.67$ MPa and $f_{c2} = -16.1$ MPa. The reinforcement stress in the out-of-plane direction was approaching yield, and the principal compressive strain, at -4.08×10^{-3}, was well into the postpeak regime. The shear stress distribution was found to be very much skewed toward the compression face. Thus, while failure of the wall ultimately resulted from crushing of the concrete on the compression face, it did so only after the elements on the tension side had essentially failed in tension-compression mode, relinquishing much of their shear-carrying capability.

The analyses also provided a measure of the importance of considering biaxial and triaxial stress effects. Ignoring the influence of nonlinear expansion and out-of-plane confinement, and thus not accounting for triaxial compression, resulted in a substantial reduction in predicted strength. The ratio of the experimental to predicted strength increased to a mean of 1.14, with a coefficient of variation of 8.2% (see Table 4). Further, the ductility at ultimate load was significantly reduced. However, there was virtually no influence on the predicted load-deformation response at low and intermediate load levels.

Conclusions

Experimental evidence has shown that, in particular cases, concrete lateral expansion (i.e., the Poisson effect) represents a significant influencing

factor in the behavior of reinforced concrete elements. Specifically, this has been found to be true for elements in tension-compression states in which the principal tensile strain is relatively small, as well as in elements subjected to biaxial or triaxial compression states. The resulting confinement effect provided by reinforcement opposing the expansion can result in significant strength enhancement and improved ductility in postultimate stress regimes.

A simple procedure was developed for incorporating concrete lateral expansion into nonlinear-elastic finite element analysis algorithms. In this procedure, material prestrains were defined and rigorously accounted for in the definition of a material stiffness matrix and element nodal forces. The procedure, used in conjunction with a secant-stiffness–based nonlinear analysis algorithm, was found to be numerically stable and able to accommodate a wide range of concrete expansion models.

To realistically represent concrete expansion and confinement effects, material models were presented describing the degree of lateral expansion, the strength degradation due to transverse cracking, the strength enhancement due to confinement, and the pre- and postultimate stress-strain responses. The strength degradation and constitutive modeling for concrete in tension-compression states were based on formulations previously presented as the modified compression field theory (MCFT). The MCFT models have been extensively corroborated with experimental data and have been shown to accurately represent behavior. The models presented for concrete expansion and for concrete constitutive response in biaxial or triaxial compression states were preliminary, used here only for the purposes of initiatory investigation; they should not be taken as proposed or recommended models.

In the examination of shear panels previously tested, the inclusion of concrete expansion in the analyses led to some improvement in the accuracy of MCFT-based models. For elements in tension-compression states in which tensile strains were relatively small, the degree of improvement in accuracy was significant. In elements experiencing high tensile strains, inclusion of concrete expansion had minimal influence on the computed response.

In the examination of shear walls tested under monotonically increasing lateral load, expansion modeling was again found to be a critical factor. When expansion was accounted for, the nonlinear finite element analyses were found to very accurately model the strength and load-deformation response of the walls. Ignoring expansion effects resulted in significantly lower strengths (by an average of 14%), and reduced ductility near ultimate load.

Work is currently under way toward the formulation of more accurate, experimentally based concrete expansion models and corresponding constitutive models.

APPENDIX I. REFERENCES

Hu, H. T., and Schnobrich, W. C. (1990). "Nonlinear analysis of cracked reinforced concrete." *Am. Concr. Inst. Struct. J.*, 87(2), 199–207.

Kupfer, H., Hilsdorf, H. K., and Rüsch, H. (1969). "Behavior of concrete under biaxial stress." *J. Am. Concr. Inst.*, 66(8), 656–666.

Lefas, I. D., Kotsovos, M. D., and Ambraseys, N. N. (1990). "Behavior of reinforced concrete structural walls: Strength, deformation characteristics, and failure mechanism." *Am. Concr. Inst. Struct. J.*, 87(1), 23–31.

Richart, F. E., Brandzaeg, A., and Brown, R. L. (1928). "A study of the failure of concrete under combined compressive stresses." *Bull. No. 185*, Univ. of Illinois Engineering Experimental Station, Urbana, Ill.

Scott, B. D., Park, R., and Priestley, M. J. N. (1982). "Stress-strain behavior of concrete confined by overlapping hoops at low and high strain rates." *J. Am. Concr. Inst.*, 79(1), 13–27.
Vecchio, F. J., and Collins, M. P. (1986). "The modified compression field theory for reinforced concrete elements subjected to shear." *J. Am. Concr. Inst.*, 83(2), 219–231.
Vecchio, F. J. (1989). "Nonlinear finite element analysis of reinforced concrete membranes." *Am. Concr. Inst. Struct. J.*, 86(1), 26–35.
Vecchio, F. J. (1990). "Reinforced concrete membrane element formulations." *J. Struct. Engrg.*, ASCE, 116(3), 730–750.
Weaver, W., Jr., and Johnston, P. R. (1984). *Finite elements for structural analysis*. Prentice-Hall, Englewood Cliffs, N.J.

APPENDIX II. NOTATION

The following symbols are used in this paper:

$\mathbf{D}_c$ = concrete material stiffness matrix;
E_1 = modulus of elasticity of orthotropic material in 1-direction;
E_2 = modulus of elasticity of orthotropic material in 2-direction;
E_{cn} = modulus of elasticity of concrete (initial tangent stiffness);
$\bar{E}_{c1}$ = secant modulus of elasticity of concrete in principal tensile stress direction;
$\bar{E}_{c2}$ = secant modulus of elasticity of concrete in principal compressive stress direction;
E_s = modulus of elasticity of reinforcing steel;
f'_c = cylinder compressive strength of concrete;
f'_t = tensile strength of concrete;
f_{c1} = largest principal tensile stress in concrete;
f_{c2} = intermediate principal stress in concrete;
f_{c3} = largest principal compressive stress in concrete;
f_{cb} = lateral confining stress on concrete;
f_{cn} = difference between normal lateral stresses on concrete;
f_{cz} = stress in concrete in out-of-plane direction;
f_p = peak compressive strength of concrete;
f_{sz} = stress in out-of-plane reinforcement;
f_{yx} = yield stress of horizontal reinforcement;
f_{yy} = yield stress of vertical reinforcement;
f_{yz} = yield stress of out-of-plane reinforcement;
F_u = ultimate lateral load capacity of shear wall;
G_{12} = shear modulus of orthotropic material relative to principal axes;
$\bar{G}_{c12}$ = secant shear modulus of concrete relative to principal axes;
K_c = strength enhancement factor for confined concrete;
v_u = ultimate shear stress of panel;
Z_m = slope of stress-strain curve for confined concrete in postultimate regime;
β = strength reduction factor for transversely cracked concrete;
γ^o_{cxy} = shear prestrain in concrete relative to x-, y-axes;
$\boldsymbol{\varepsilon}^o_c$ = concrete prestrain matrix;
ε_{c1} = largest principal strain in concrete;
ε_{c2} = intermediate principal strain in concrete;
ε_{c3} = largest principal compressive strain in concrete;
ε^o_{c1} = prestrain in concrete in principal tensile direction;

ε_{c2}^{o} = prestrain in concrete in principal compressive direction;
ε_{cz} = strain in concrete in out-of-plane direction;
ε_{cx}^{o} = prestrain in concrete in horizontal direction;
ε_{cy}^{o} = prestrain in concrete in vertical direction;
ε_{o} = strain in concrete cylinder at stress f_c';
ε_{p} = strain in concrete at peak stress f_p;
θ = angle of inclination of principal stresses in concrete;
ν_{o} = initial value of Poisson ratio;
ν_{12} = Poisson ratio describing strain in 1-direction due to compressive stress in 2-direction;
ν_{12}^{e} = elastic component of ν_{12};
ν_{12}^{*} = residual component of ν_{12};
ν_{21} = Poisson ratio describing strain in 2-direction due to compressive stress in 1-direction;
ρ_{x} = steel reinforcement ratio in horizontal direction;
ρ_{y} = steel reinforcement ratio in vertical direction; and
ρ_{z} = steel reinforcement ratio in out-of-plane direction.